J. Phys. Chem. A **2007,** *111,* 10075−10083

Vacuum Ultraviolet (VUV) Photoionization of Small Water Clusters

Leonid Belau,[†] Kevin R. Wilson,[†] Stephen R. Leone,[†,‡] and Musahid Ahmed*,[†]

Chemical Sciences Division, Lawrence Berkeley National Laboratory, Berkeley, California 94720, and Departments of Chemistry and Physics, University of California—Berkeley, Berkeley, California 94720

Received: July 5, 2007

Tunable vacuum ultraviolet (VUV) photoionization studies of water clusters are performed using 10−14 eV synchrotron radiation and analyzed by reflectron time-of-flight (TOF) mass spectrometry. Photoionization efficiency (PIE) curves for protonated water clusters $(H_2O)_nH^+$ are measured with 50 meV energy resolution. The appearance energies of a series of protonated water clusters are determined from the photoionization threshold for clusters composed of up to 79 molecules. These appearance energies represent an upper limit of the adiabatic ionization energy of the corresponding parent neutral water cluster in the supersonic molecular beam. The experimental results show a sharp drop in the appearance energy for the small neutral water clusters (from 12.62 ± 0.05 to 10.94 ± 0.06 eV, for H_2O and $(H_2O)_4$, respectively), followed by a gradual decrease for clusters up to $(H_2O)_{23}$ converging to a value of 10.6 eV (±0.2 eV). The dissociation energy to remove a water molecule from the corresponding neutral water cluster is derived through thermodynamic cycles utilizing the dissociation energies of protonated water clusters reported previously in the literature. The experimental results show a gradual decrease of the dissociation energy for removal of one water molecule for small neutral water clusters ($3 \leq n \leq 9$). This dissociation energy is discussed within the context of hydrogen bond breaking in a neutral water cluster.

Introduction

There is enormous interest in the properties of water both from a fundamental point of view and from the importance of water in biological and atmospheric processes on Earth. Water in its various physical states—gas, liquid and ice—have been studied with a variety of experimental and theoretical techniques, and recently the studies of the structure of liquid water have sparked a vigorous debate regarding the coordination of water in its liquid state.[1−4] The use of clusters as a vehicle for studying molecular properties allows for systematic investigations of how bulk properties of a substance arise from the isolated molecule as the cluster size is increased.

Optical spectroscopy is typically applied to probe neutral water clusters following the seminal work of Saykally and co-workers,[5−8] whereas Lee and co-workers pioneered the study of the structure of ionic water clusters with IR spectroscopy.[9,10] The size dependent spectroscopic properties of neutral water clusters were studied with VUV[11] and IR[12] spectroscopic methods. In addition, a substantial effort was invested in probing the structure of protonated water clusters utilizing IR vibrational spectroscopy.[13,14] One aspect of this work stems from trying to understand the properties of $(H_2O)_{21}H^+$, whose magic-number-like behavior was reported first by Lin in 1973.[15] Searcy and Fenn in 1974[16] suggested that this arises from the formation of a very stable dodecahedral cluster structure, and this was confirmed recently by Shin et al.[13] and Miyazaki et al.[14] Moreover, the chemical structures of small protonated water clusters have been the subject of many experimental and theoretical investigations. It is established that two main structures, “Eigen” (H_3O^+)[17] and “Zundel” $(H_5O_2{}^+)$[18] play an important role in large water cluster structures. In this work we do not experimentally resolve these two prominent water cluster structure types, and therefore, *n*-mer protonated water clusters will be denoted as $(H_2O)_nH^+$.

Supersonic expansion techniques[19,20] provide a convenient way to generate a pulsed or continuous molecular beam of water clusters of different sizes. Using this technique, water clusters approach internal temperatures of 130−180 K, such temperatures being relevant in the Earth’s mesosphere.[21,22] The ionization properties of water clusters, readily created in these molecular beams, are intensively studied by mass spectrometric methods utilizing different ionization techniques: single-photon ionization,[23−26] electron impact ionization,[27] chemical ionization,[28,29] and femtosecond multiphoton ionization.[30] Recently there is a resurgence of negatively charged water cluster studies using mass spectroscopic techniques with an eye to understanding where a solvated electron is located.[31−33] In these studies, electron attachment to water clusters in the supersonic molecular beam creates clusters of the type $(H_2O)_n^-$ but also gives rise to $(H_2O)_nO^-$.[34]

Photoionization of neutral water clusters creates unstable cations, $[(H_2O)_n]^+$, which undergo very fast intracluster charge redistribution on the subpicosecond time scale.[35] The most thermodynamically and kinetically favorable reaction pathway is proton transfer and subsequent $OH^\bullet$ loss as summarized in eq 1.

$$(H_2O)_n + h\nu \rightarrow [(H_2O)_n]^+ + e^- \rightarrow (H_2O)_{n-1}H^+ + OH^\bullet + e^- \quad (1)$$

Therefore, it is the protonated water clusters, $(H_2O)_nH^+$, with the exception of the neutral water monomer ($n = 1$) and dimer ($n = 2$), that become the dominant peaks in almost all mass

---

* Corresponding author. Phone: (510) 486-6355. Fax: (510) 486-5311. E-mail: MAhmed@lbl.gov.

[†] Lawrence Berkeley National Laboratory.

[‡] University of California—Berkeley.

10.1021/jp075263v CCC: $37.00

spectrometric studies of water clusters employing various ionization techniques.[23−26,28,29]

After the initial fast protonated cluster formation, a relatively slow water molecule evaporation process can take place within the mass spectrometer. This is because these protonated water clusters are usually created with small amounts of internal energy, and they tend to evaporate water molecules to reduce this energy. This process is shown in eq 2.

$$(H_2O)_{n-1}H^+ \rightarrow (H_2O)_{n-2}H^+ + H_2O \qquad (2)$$

There are some cases where water clusters of type $(H_2O)_n^+$ can be formed by employing a supersonic expansion of Ar at high pressures, leading to formation of heterogeneous Ar:water clusters.[25,36] In this case, rapid evaporative cooling of Ar atoms following photoionization leads to the effective cooling of the internal energy of the ionized water cluster. Thus, the evaporative cooling of Ar atoms from the cluster quenches $OH^•$ loss, leading to formation of unprotonated water clusters, $(H_2O)_n^+$, possessing minimal internal energy.

Wei and Castleman published a comprehensive study of the metastable fragmentation of protonated water clusters employing a chemical ionization method. A careful and systematic study of the time-of-flight trajectories of the parent and daughter metastable clusters helped these authors decipher the kinetics and dynamics of this process.[29] They showed that the binding energy of weakly bound clusters as well as other thermodynamic properties of protonated water clusters can be evaluated by analyzing the decay fraction of parent versus metastable daughter fragments and employing the Klotz evaporative cooling model.[37]

Photoionization efficiency (PIE) studies of relatively small water clusters were performed earlier with He and H_2 lamps and tunable synchrotron VUV radiation.[24,26,38] Using single-photon ionization, Ng et al.[24] reported appearance energies (AE) for small water clusters formed from $(H_2O)_2$ photoionization: 11.73 ± 0.03 and 11.21 ± 0.09 eV for H_3O^+ and $(H_2O)_2^+$, respectively. Shiromaru and co-workers[26] reported AEs of 10.87 ± 0.06 and 10.92 ± 0.04 eV for $(H_2O)_2^+$ and $(H_2O)_3^+$, from $(H_2O)_2$ and $(H_2O)_3$, respectively. Moreover, they also reported the AEs for $(H_2O)_2H^+$ and $(H_2O)_3H^+$ formed from $(H_2O)_3$ and $(H_2O)_4$ photoionization to be 11.18 ± 0.02 and 11.10 ± 0.02 eV, respectively.[26] Apart from the work mentioned above, to the best of our knowledge, there are no experimental determinations of the appearance energies for protonated water clusters larger than the 3-mer ($(H_2O)_3H^+$). Following these pioneering studies performed over a decade ago, there are no systematic studies of the VUV photoionization properties of water clusters apart from a recent study of water clusters with fixed wavelength radiation.[23] In that work, Dong et al.[23] photoionized water clusters with 26.5 eV laser generated radiation and studied the resulting fragmentation dynamics utilizing reflectron mass spectrometry. They suggested that a small fraction of the photon energy is deposited in the cluster for metastable dissociation of the resulting ions, and the departing electron removes most of the excess energy.

In the present work, small water clusters, generated in a supersonic expansion, are photoionized utilizing tunable VUV radiation produced by a synchrotron. The resulting protonated cluster ions are studied with a reflectron TOF mass spectrometer. The total ion intensity of protonated clusters and their metastable fragment water clusters allows for the determination of the relative abundance of the neutral water clusters for $3 \leq n \leq 48$. AEs for the protonated water clusters up to $(H_2O)_{79}H^+$ are measured experimentally. These results provide new insight on the hydrogen bonding of neutral water clusters.

Experimental Setup

The experiments are performed in a chamber incorporating a continuous supersonic expansion of water vapor to produce water clusters. The apparatus is coupled to a 3 meter vacuum monochromator on the Chemical Dynamics Beamline (9.0.2) located at the Advanced Light Source. This apparatus is recently discussed for different experiments[39] and relatively minor changes are introduced, such as to produce a continuous supersonic molecular beam of the water clusters. This modification allows an improvement in the experimental duty cycle from 1 kHz up to 10 kHz, substantially improving the signal-to-noise ratio.

Neutral clusters are formed in a supersonic expansion of 101 kPa of Ar with seeded water vapor (liquid water maintained at 298 K giving rise to 3.2 kPa vapor pressure) through a 100 μm nozzle orifice and pass through a 1 mm conical skimmer (Beam Dynamics, Inc.) located 20 mm downstream. The pressures in the source and main chambers are below 2.7×10^{-3} and 2.7×10^{-5} Pa, under normal operating conditions. In the main chamber, the neutral water cluster beam is interrogated in the ionization region of a commercial reflectron mass spectrometer (R. M. Jordan) by tunable undulator VUV radiation. Since the synchrotron light is quasicontinuous (500 MHz), a start pulse for the TOF ion packet is provided by pulsing the ion optics electric potential. The accelerator and repeller plates of the ion optics are biased at the same potential (1600 V), and ions are extracted by employing a fast switching (100 ns rise time) of the repeller plate to 1800 V with a dwell time of 5 μs. Ions are accelerated perpendicularly to their initial velocity direction through the field free region toward the reflectron. Ions, reflected in the 21 stage electrostatic field of the ion mirror, are detected by a 25 mm diameter microchannel plate (MCP) installed at the end of the second field free region. The time-dependent electrical signal from the MCP is amplified by a fast preamplifier (Ortec, VT120A) and collected by a multichannel-scalar card (FAST-Comtec, P7886) and integrated with a PC computer running LABVIEW 6.0 software (National Instruments). Time-of flight spectra are recorded for the ionization photon energy range between 10 and 14 eV. The typical photon energy step size used for these experiments is 50 meV, and the accumulation time at each photon energy is 300 s. The photoionization efficiency (PIE) curves of the water clusters are obtained by integrating over the peaks in the mass spectrum at each photon energy and normalized by the photon flux. The synchrotron VUV photon flux is measured by a Si photodiode (IRD, SXUV-100). In this research, we use triply purified water, with resistivity >18 MΩ.

Results

A typical reflectron TOF mass spectrum of gas-phase water clusters seeded in Ar is shown in Figure 1. Three series of peaks comprising unprotonated and protonated water clusters and their metastable fragments can be distinguished in this spectrum; however, only two unprotonated water species corresponding to H_2O^+ and $(H_2O)_2^+$ are observed. Protonated water clusters are created as a result of rapid intramolecular charge redistribution with subsequent $OH^•$ elimination from the photoionized cations.

A detailed analysis of metastable fragmentation of protonated clusters has been published by Wei and Castleman[29] and aids in deciphering the complicated mass spectra that arise from

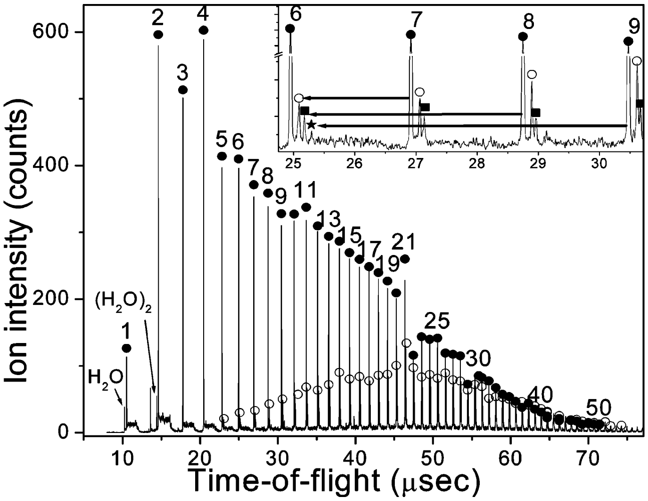

Figure 1. Time-of-flight mass spectrum of water clusters, formed by continuous co-expansion of water with Ar at 1 bar backing pressure. Ionization is performed with 12.5 eV light. (Insert) Small protonated water clusters consisting of $n = 6-9$ shows the relative abundance of protonated and metastable water clusters. The filled circles (●) indicate peaks associated with non-fragmented protonated water clusters ($(H_2O)_nH^+$), open circles (○), squares (■), and stars (★) denote metastable fragments of the protonated water clusters due to single, double, and triple water molecule loss, respectively (as marked in the insert figure).

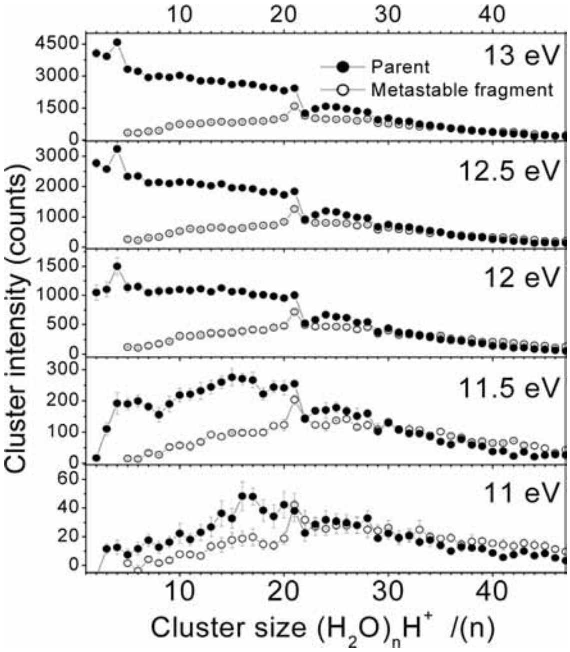

Figure 2. Intensity of protonated water clusters ($(H_2O)_nH^+$) (filled circles, ●) and their metastable daughter fragments (open circles, ○) from one water molecules loss, described by eq 2 at different photon energies denoted in each panel.

VUV photoionization of water clusters. In our case, three main metastable series can be distinguished, as indicated in the insert of Figure 1. The enlarged section of clusters $n = 6-9$ is used to explain the metastable peak assignments. The filled circles represent nonfragmented protonated water cluster ions, whereas the open circles, squares, and stars represent metastable fragment clusters undergoing one, two, and three water monomer evaporation, respectively, from the protonated cluster ion in the drift tube. The metastable fragment cluster ions, created in the field-free region, can be easily discriminated in the reflectron section of the TOF mass spectrometer since they appear as satellites to the main unfragmented protonated cluster ion peaks.

The mass spectra of water clusters are recorded utilizing VUV synchrotron radiation in the region of 10−13 eV photon energies in steps of 0.05 eV. The relative signal intensity of the protonated water clusters and their metastable daughter fragments upon one water molecule loss at five different ionization energies are shown in Figure 2. The filled points in Figure 2 represent the relative intensity of parent protonated water clusters, and the open points are the metastable daughter fragments (from one water molecule loss), which are obtained by integrating over the peak in the mass spectrum at each photon energy.

Figure 2 shows that the water cluster distribution signal intensities depend on the photoionization energy. In general, the detection efficiency of the MCP is dependent on the ion velocity and the properties of the MCP itself. In this experiment, ions are accelerated up to 1.8 kV and we assume that the detection efficiency of our apparatus is relatively flat for ions up to $m/z < 2000$. Hence, the relative intensities of water cluster signals, shown in Figure 2, should reflect the photoionization efficiency of the water clusters.

At low photon energies (≤11 eV), the cluster distribution of the protonated water cluster peaks at $n = 17$ (m/z 307), with relatively lower intensities of small and large protonated clusters, $n < 10$ and up to $n = 50$, respectively. At photon energies >11 eV, the cluster distribution gradually changes, and the smaller protonated clusters become more prominent. In the region of small protonated clusters $2 \leq n \leq 8$, a magic number of $n = 4$ is easily discerned compared to other peaks. The discontinuity of the protonated water cluster, $n = 4$, was observed earlier by Lancaster et al.[40] and by Dong et al.[23] In the region of larger clusters ($n > 8$), there is a pronounced discontinuity at 21 water molecules ($(H_2O)_{21}H^+$), revealing a clear irregularity in the otherwise smooth cluster distribution. The drop in relative intensity at $n = 22$ may arise from enhanced metastable fragmentation of this particular cluster leading to the formation of the more stable protonated water cluster $(H_2O)_{21}H^+$. The relative intensity of clusters greater than $n = 22$ drops significantly when compared to the smaller clusters.

The distribution of metastable fragments looks significantly different from their parent protonated water clusters for cluster size $n < 20$. However, at all photon energies, the metastable fragment cluster distribution looks very similar, broadly peaked around 20 water clusters, with $n = 21$ showing up as a magic number. Because the metastable fragmentation rate of small protonated water clusters is very low, the relative intensity of small metastable daughter fragments even at high photon energies is lower than that for large clusters ($n > 10$). It is interesting to note that the cluster distributions displayed in Figures 1 and 2 are similar to those reported by other experimentalists, utilizing single-photon ionization at 26.5 eV[23] and chemical ionization.[29] This suggests that in all these experiments the formation of protonated water clusters and subsequent metastable fragmentation is the dominant process that dictates the overall mass spectral distributions, irrespective of the initial ionization process.

The ratio of metastable fragmentation of the protonated water cluster in the field-free region of the mass spectrometer is denoted as the decay fraction: $D = I_M/(I_M + I_P)$, where I_M is the total of all metastable fragment intensities (from loss of one, two, or three water molecules) in the mass spectrum and I_P is the protonated parent cluster intensity. The decay fraction analysis provides a convenient way to quantify relative evaporation energies for protonated water clusters.[29,37] In this work, the tunability of VUV light provides an excellent tool for the

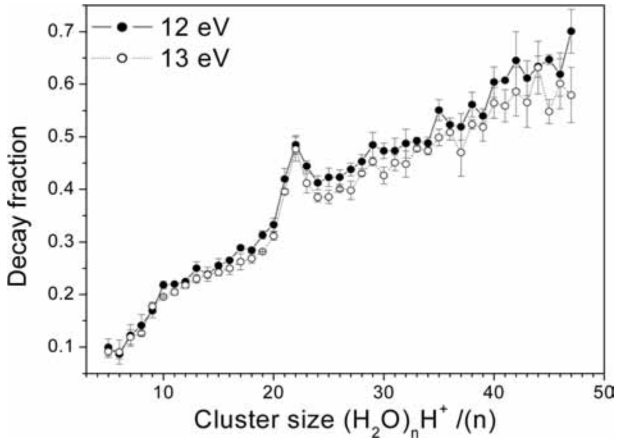

Figure 3. Decay fraction $D = I_M/(I_M + I_P)$ of metastable fragmentation of protonated water clusters ($(H_2O)_nH^+$) in the molecular beam as function of cluster size at 12 (●) and 13 eV (○). The error bars represent the standard deviations of three data sets.

systematic study of the decay fraction with photon energy in the range 10−14 eV and allows us to describe the differences in the metastable fragmentation as a function of the cluster size and ionization energy. Two representative curves are shown in Figure 3.

There are very minor differences between the decay fractions *D* (Figure 3) at these two photon energies with the curve at 13 eV being slightly lower than at 12 eV, but this difference is less than the error bars. The decay fraction curve at 11 eV has a poorer signal-to-noise ratio (not shown); however, it follows the same trend with photon energy as the curves for 12 and 13 eV. Moreover, the decay fraction at photon energies above 11 eV exhibit the same slope as shown in Figure 3 for 12 and 13 eV. These results agree very well with those reported by Shi et al.[28] and Dong et al.[23] in their ranges of clusters of $4 < n < 24$; the results follow the same slope and display a prominent magic number at $n = 22$. However, the absolute ratio is somewhat smaller in our work. Shi et al.[28] (chemical ionization) and Dong et al.[23] (single-photon ionization at 26.5 eV) reported the decay fraction of metastable fragmentation of protonated water cluster $(H_2O)_{22}H^+$ to be $D_{22} \approx 0.8$, in contrast to our result, where $D_{22} = 0.48 \pm 0.02$ is obtained at 12 and 13 eV. The smaller decay fraction suggests less metastable fragmentation occurs in the drift region. This could arise from threshold photoionization, which deposits less excess energy into the clusters in current work. In contrast to the cluster distribution mass spectrum in Figures 1 and 2, where the magic number in the range of large protonated water clusters is at $n = 21$, the magic number in the decay fraction curve represents the cluster with the highest metastable fragmentation ratio ($n = 22$).

The photoionization efficiency (PIE) curves of protonated water clusters are obtained by integrating the corresponding ion peaks in the mass spectrum as a function of photon energy. The mass resolution of our apparatus is optimized to distinguish protonated clusters from their metastable daughter fragment clusters up to $n = 47$ ($(H_2O)_{47}H^+$) and to resolve metastable water clusters up to $n = 79$.

The PIE curves for H_2O^+ from H_2O, and $(H_2O)_2{}^+$ and H_3O^+ from $(H_2O)_2$, agree very well with those reported earlier by Ng et al.[24] The PIE curves of H_2O^+ and H_3O^+ (from H_2O and $(H_2O)_2$ photoionization) gradually rise after the photoionization onsets of 12.62 ± 0.05 and 11.74 ± 0.05 eV, respectively, and show no distinct vibrational structure with photon energy, as noted by Ng et al.[24] These onsets can be compared to those measured by Ng et al.[24] (12.601 ± 0.009 and 11.73 ± 0.03 eV for H_2O^+ and H_3O^+, respectively). Moreover, the PIE curve corresponding to $(H_2O)_2{}^+$ does show the same vibrational structure as reported previously by Ng et al.[24] Our onset value of 11.25 ± 0.05 eV is also in excellent agreement with the 11.21 ± 0.03 eV value measured by Ng et al.[24] However, the PIE spectra of $(H_2O)_2{}^+$ and other small protonated water clusters, $(H_2O)_2H^+$ from $(H_2O)_3$ and $(H_2O)_3H^+$ from $(H_2O)_4$, exhibit different spectral curvatures and photoionization onsets than those reported earlier by Shiromaru et al.[26] They reported AE values of 10.87 ± 0.06, 11.18 ± 0.02, and 11.10 ± 0.02 eV, for $(H_2O)_2{}^+$, $(H_2O)_2H^+$, and $(H_2O)_3H^+$, respectively.[26] These values are significantly lower than those reported earlier by Ng et al.[24] and observed in the current work. The reason for this discrepancy could be from possible contributions to the parent ion peak intensity from other species, possessing lower ionization onsets. As was reported by Shiromaru et al. the high stagnation pressure of Ar in that work increases the concentration of heterogeneous clusters of type $Ar_x{:}(H_2O)_y$.[26] It is plausible that the ionization energies of these clusters is somewhat lower, taking into account the known bathochromic shift of Ar in van der Waals clusters. The rapid evaporation of Ar atoms from the photoionized cluster $Ar_x(H_2O)_nH^+$, inside the ionization region of the Shiromaru et al. quadrupole mass spectrometer could alter the ion thresholds.[26]

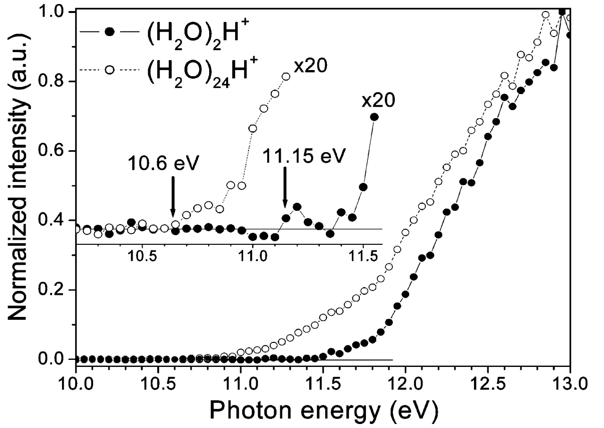

Figure 4. Normalized PIE curves of two parent protonated water clusters performed under the same experimental conditions: $(H_2O)_2H^+$, filled circles (●); and $(H_2O)_{24}H^+$, open circles (○). The insert shows × 20 expanded vertical scale. The arrows indicate the photoionization onset: 11.15 ± 0.05 and 10.6 ± 0.1 eV for $(H_2O)_2H^+$ from $(H_2O)_3$ and $(H_2O)_{24}H^+$ from $(H_2O)_{25}$, respectively.

The PIE curves of the small and large protonated water clusters exhibit a fairly smooth and structureless curvature above the photoionization threshold. The PIE curves of larger protonated water clusters are significantly shifted to lower energies compared to the smaller analogs. This is seen clearly in Figure 4 by comparing the two PIE spectra for parent protonated water clusters $(H_2O)_2H^+$ and $(H_2O)_{24}H^+$.

The AE values of the protonated water clusters are determined by the photoionization signal onset of the corresponding peaks in the mass spectrum as a function of the photon energy. In other words, the first point of a PIE curve above the background level is taken to be the AE value. The AE values for $(H_2O)_2H^+$ and $(H_2O)_{24}H^+$ are displayed in Figure 4 by the arrows. Examining the onsets for $(H_2O)_2H^+$ and $(H_2O)_{24}H^+$, it is clearly evident that there is a shift upon moving from the 2-mer to the 24-mer cluster. The AE of $(H_2O)_2H^+$ from $(H_2O)_3$ is 11.15 ± 0.05 eV, which is 0.55 eV higher than the onset for $(H_2O)_{24}H^+$ from $(H_2O)_{25}$ (10.6 ± 0.1 eV).

The PIE curves for metastable fragment clusters are obtained in the same way as their nonfragmented parent cations, by

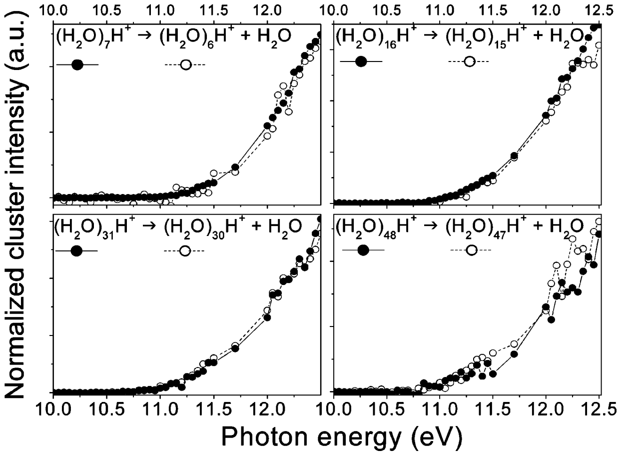

Figure 5. PIE spectra comparison of four different protonated water clusters to their ($n - 1$) metastable fragments (loss of one water molecule): $(H_2O)_7H^+$, $(H_2O)_{16}H^+$, $(H_2O)_{31}H^+$, and $(H_2O)_{48}H^+$. Filled circles (●) denote nonfragmented protonated water clusters, and open circles (○) correspond to the first metastable daughter cluster ions created due to single water molecule loss.

integrating over the mass spectral peak intensities, as a function of the photon energy. There are only minor differences in the PIE curve profiles for protonated clusters and their corresponding metastable daughter fragments in the cluster region of $4 \leq n \leq 47$, and results are shown in Figure 5 for four representative cluster sizes.

The close correspondence of the PIE curves of the parent protonated water clusters and their metastable fragments suggests that a water monomer loss, as shown in eq 2, is not involved directly in the photoionization process and is taking place later in time. This close correspondence is a confirmation of the data shown in Figure 3 (for 12 and 13 eV), where the relative intensities of the parent protonated water cluster and its metastable fragment are the same, irrespective of photon energy.

Typically, in photoionization mass spectrometry, a least-squares fit to the change of slope versus photon energy at the origin and extrapolation of this fit to zero ionization yield allows for the determination of the ionization energy. We assume the neutral water cluster is cold ($T = 160 \pm 40$ K)[20,23,41,42] and therefore the internal energy is low. This assumption is based on the similarity of our cluster generation conditions and the mass spectral patterns obtained in this work and compared to those reported previously in the literature. An unequivocal determination will require spectroscopic mapping of the internal energy distributions, which is presently not possible. In the case of cluster photoionization, the small gap between many close-lying vibrational states in the cation can significantly congest the photoionization onset making an accurate determination difficult. In addition, the Franck−Condon factors and possible lack of a clean vertical photoionization onset can further complicate the analysis. Therefore, the appearance energies measured here are considered to be an upper limit for the true adiabatic ionization energy of corresponding neutral water clusters.

The intensities of protonated water clusters greater than 47 molecules are below the detection limit of our apparatus since they fragment in the drift tube. However daughter metastable fragment protonated water clusters are discerned up to $n = 79$. Therefore, the PIE curves of protonated water clusters $47 < n \leq 79$, are obtained from the daughter, metastable fragmented clusters, as described in eq 2. As is shown in Figure 5, these curves are very similar, allowing us to establish appearance energies of protonated water clusters in the expanded size range of $4 \leq n \leq 79$ (as is discussed below).

Discussion

The photoionization mass spectra at all photon energies below the ionization onset of the water monomer (12.6 eV) are dominated by protonated water clusters ($(H_2O)_nH^+$). Neutral water clusters are photoionized on a very fast time scale producing cations with a strained geometrical configuration in the corresponding ion state. This cation subsequently undergoes substantial reorganization accompanied by $OH^\bullet$ elimination in order to obtain a preferred positive charge stabilization.[30,35] Although the $OH^\bullet$ elimination and structural rearrangement step has not been observed experimentally, it is inferred through available structural information. Theoretical calculations suggest that the average distance between two neighboring oxygen atoms (the radial distribution function for O−O distances) is substantially shorter in protonated water clusters than in their neutral forms.[43,44] For example, the O−O distances in the neutral dimer, cyclic trimer, and tetramer are 2.976,[5] 2.845,[45] and 2.782 Å,[45] respectively, while shrinking to almost 2.5 Å in the corresponding protonated forms.[46] Based on theoretical calculations and experimental evidence, the mean O−O distance between neighbor molecules in larger water clusters shrinks from 2.75 Å in the neutral state to almost 2.5 Å for the protonated water cluster ($2 \leq n \leq 100$).[47,48] In comparison, the mean O−O distance between neighbor molecules in liquid water is 2.85 Å at 298 K and 2.785 Å at 183 K for hexagonal ice I_h, and 2.76 Å at 10 K for amorphous ice.[48−52]

The O−O distance change between two neighboring water molecules in a water cluster can characterize a Franck−Condon overlap during the process of single photon ionization. According to theoretical calculations by Barnett and Landman the O−O distance in the water trimer ($(H_2O)_3$) shrinks from 2.89 Å in the neutral form to 2.47 Å in its cationic form ($(H_2O)_3^+$).[53] The tetramer and pentamer show similar trends of O−O distance shortening, which is also anticipated in larger water clusters. This would suggest that the Franck−Condon overlap for direct photoionization from neutral $(H_2O)_n$ to $(H_2O)^+{}_n$ may be small.

Ionized water clusters undergo rapid intracluster proton-transfer reaction followed by concomitant $OH^\bullet$ loss and formation of a protonated water cluster. Theoretical calculations performed by Tachikawa report that the photoionized trimer and tetramer neutral water clusters show clear separation of $OH^\bullet$ after 25 and 180 fs, respectively.[35] Recent calculations of $(H_2O)_{17}$ photoionization dynamics show that even large water clusters lose $OH^\bullet$ on similar time-scales.[54] Due to the relatively small extraction potentials (160 and 1280 V/cm electrostatic field strength in two acceleration regions) employed in this work, the water clusters reside for 1−7 μs (depending on the cluster size) inside the acceleration region of the mass spectrometer. This would suggest that the protonated water clusters are formed, following single photon ionization, inside the acceleration region of our apparatus.

The distribution of protonated water clusters and their metastable daughter fragments do not change as a function of the photon energy (>12 eV, Figure 2). At these photon energies (>12 eV), almost all water clusters are ionized (except the monomer). There are no experimental data or theoretical predictions for the photoionization cross-section of neutral water clusters. We assume a constant detection efficiency and ionization probability for small and large water clusters. Thus, the sum of the intensity of the parent protonated water cluster and the corresponding daughter metastable fragment should represent

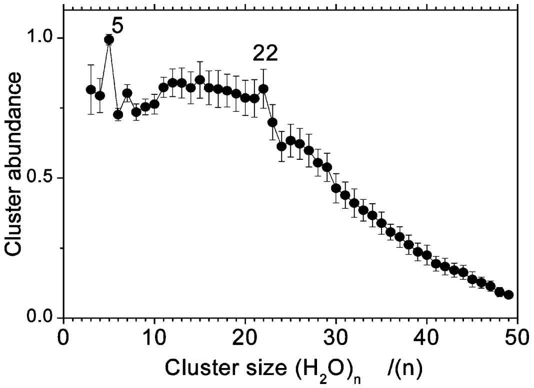

Figure 6. Size dependent normal abundance of water clusters $(H_2O)_n$ in the supersonic molecular beam. This is a sum of the experimentally measured values of the stable and metastable ions of a given cluster size and assumes equal ionization efficiencies for all cluster sizes. The error bars represent the standard deviations over 7 data sets and ion intensity integration for photon energies in the range of 12−13 eV.

the neutral water cluster abundances in the supersonic molecular beam, which is shown in Figure 6 at 13 eV photon energy.

The curve in Figure 6 is an average of normalized neutral water cluster abundances over all photon energies in the range of 12−13 eV for 7 separate data sets. There is one prominent magic number in Figure 6 at $n = 5$, demonstrating that $(H_2O)_5$ is formed with extraordinary stability due to its favorable geometry. The water pentamer is the largest stable cyclic structure with O−O−O bond angles of 108° with almost linear hydrogen bond angles (O−H−O) and O−O distance close to 2.76 Å. Although the structure of the tetramer is cyclic, the O−O−O and O−H−O angles are not as favorable as in the case of the water pentamer which possess the H-bonding tetrahedral geometrical properties of the monomer very similar to liquid and ice.

The observed decrease of the hexamer abundance relative to the pentamer, in supersonic jet expansions of water, has been noted previously.[55,56] Hermann et al. observed a discontinuity of the protonated water cluster distribution in the supersonic molecular beam from $n = 4$ to 5; however, the result was dependent on the stagnation pressure.[55] Another observation of enhanced abundance of the pentamer when compared to the hexamer is from the work of Nauta and Miller.[56] They compared the IR spectra of small neutral water clusters formed in a supersonic jet expansion to those confined within ultracold helium droplets. The most striking observation, which is derived by comparing the intensity of O−H stretching modes, was that the cyclic neutral water hexamer was not abundant at all in the supersonic beam.[56] The relative distributions of the water clusters are not unique and will vary with the temperature of the neutral beam; future experiments with careful control of the internal energy of the cluster beam can allow us to study systematic trends.

The neutral water cluster $n = 22$ is more abundant than $n =$ 21 or 23; however, the error limits do not allow us to state this with absolute certainty. The rapid decrease in abundance for neutral clusters larger than $n = 22$ would suggest that the second solvation shell influences the distribution in the molecular beam. This probably arises from the weaker hydrogen bonding as has been discussed recently by Shin et al.[13] and Miyazaki et al.[14] for protonated water cluster distributions.

The relative intensities of protonated water clusters and corresponding PIE curves are not affected by the metastable cluster fragmentation of one or more water monomers (as described in eq 2). First, the decay fraction during the cluster extraction in the acceleration region of the TOF is very small. The flight time of ions in this region is much smaller in comparison to the flight time in the field-free region. Since the decay fraction of small protonated water clusters ($n < 20$) is less than 0.3 (see Figure 3), we anticipate even less decay to occur during the ion acceleration time. It is not possible to measure the decay fraction during the acceleration, because in this case the flight trajectory of the parent and the daughter clusters will be very similar and no temporal separation is anticipated between parent and daughter metastable fragment. However, from available data we can estimate this value. Taking into account the strength of the acceleration electric field (160 and 1280 V/cm), the typical time-of-flight of a 21-mer protonated water cluster ($(H_2O)_{21}H^+$) in the acceleration region of our apparatus is calculated to be 2.7 μs. According to the work of Dong et al., the metastable fragmentation rate constant is about 15 000 s^{-1} for a 21-mer protonated water cluster.[23] We assume that the rate is lower in our case, because of lower photon energies that result in lower absolute values of the decay fraction. Therefore 15 000 s^{-1} is the upper limit for metastable fragmentation for a 21-mer protonated water cluster in our experiment. From this, we estimate that less than 4% of 21-mer protonated clusters are fragmented in the acceleration region of our apparatus. This ratio is even lower for the smaller clusters.

Moreover, an asymmetric peak broadening, tailing to longer TOF, is not observed for peaks in the mass spectrum in the region of protonated water clusters $1 < n < 30$, suggesting that metastable fragmentation during cluster acceleration is not the dominant fragmentation process. Additionally, metastable fragmentation in the field-free region of the TOF apparatus is well resolved in the reflectron ion mirror by separating parent and daughter protonated water clusters. This is exactly what is shown in Figure 1. Protonated water clusters larger than $n > 40$ fragment faster and travel longer in the acceleration region. Thus, the larger protonated water cluster relative intensities have an additional component from metastable fragmentation inside the acceleration region. For example almost 10% from the 40-mer and more than 20% from the 70-mer protonated water clusters fragment during the acceleration, evaporating at least one water molecule.

The decay fraction of metastable fragmentation, reported in Figure 3, is lower than those previously reported by Shi et al.[28] and Dong et al.,[23] suggesting that lower energy light and better cooling conditions in the molecular beam in our work result in less fragmentation. The results suggest that the 4% fragmentation for the 21-mer protonated water clusters observed in this work is probably an upper limit. Furthermore, due to the very insignificant AE fluctuations for clusters $n > 20$ (see Figure 7), one can conclude that metastable fragmentation inside the acceleration region should not considerably affect the photoionization onset of the protonated water cluster.

The rapid loss of $OH^\bullet$ from photoionized water clusters, together with the small ratio of the metastable fragmentation in the acceleration region (for $n < 30$) and similar decay fractions (D) of protonated water clusters at all photon energies allow us to make the following assertion. The ionization energies of the parent neutral water clusters ($(H_2O)_n$) are being mapped onto the appearance energies of the positively charged protonated, daughter clusters ($(H_2O)_{n-1}H^+$), which are obtained experimentally from the PIE curves in our experiment. Figure 7 represents the AE values for protonated water clusters as a function of their size obtained from the photoionization onsets of the PIE curves. In light of the arguments made above, Figure 7 displays the size dependent appearance energy distribution of the neutral

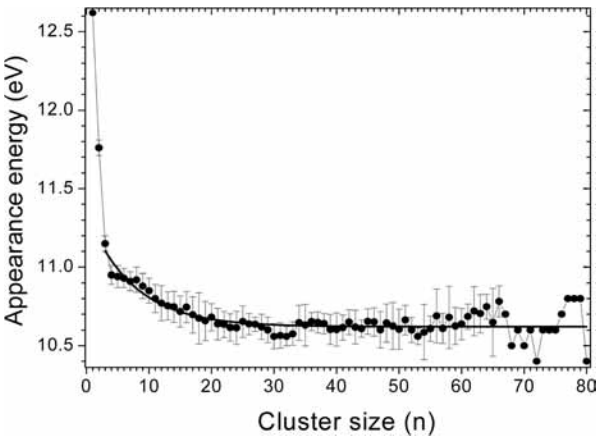

Figure 7. Size dependent appearance energy of neutral water clusters $(H_2O)_n$, derived from the appearance energy observation of daughter protonated water clusters. The error bars indicate the photoionization onset uncertainty of 7 different experimental data sets. The actual numerical values are available in the Supporting Information (Table A). The single-exponential fitting line is reported for clusters $3 \leq n \leq 80$ and shows asymptotical behavior converging to 10.6 ± 0.2 eV.

water clusters. The energies reported here are most likely upper limits to the true adiabatic ionization energy.

It is immediately apparent that the appearance energy distribution of the neutral water clusters, shown in Figure 7, can be separated into two parts; a rapid drop from 12.62 ± 0.05 (H_2O) down to 10.94 ± 0.06 eV ($(H_2O)_4$). Then the appearance energy values of the larger clusters, up to $(H_2O)_{23}$ ($5 \leq n \leq 23$), show a very gradual decrease that converges to a value of 10.6 ± 0.1 eV for $n > 23$. The appearance energy values of neutral water clusters, larger than $(H_2O)_{23}$, do not show significant changes, exhibiting small fluctuations around 10.6 ± 0.2 eV. To the best of our knowledge, this is the first experiment to determine the appearance energies of neutral water clusters for $5 \leq n \leq 80$. Winter et al.[57] discuss the photoionization threshold of liquid water in the context of electron emission from VUV irradiated liquid water beams. They measure an energy of 9.9 eV for the ionization onset, which is much lower than the convergence values measured in our work. Our determinations are derived from photoionization mass spectrometry measurements where ionization onsets are used to derive an appearance energy, whereas in the liquid studies, it is the photoelectron measurement that is used to derive the ionization energy.

It is significant that the appearance energies converge around 10.6 eV for clusters above $(H_2O)_{20}$. The 21-mer protonated water cluster ($(H_2O)_{21}H^+$) is a well-known magic number that was observed under a variety of different ionization conditions (electron impact, multiphoton ionization, chemical ionization, femtosecond photoionization, etc.) and was attributed to the formation of a very stable geometrical dodecahedron form.[15,27,28,30] Previous experimental and theoretical studies show that protonated water clusters for $n > 21$ have different IR absorption properties when compared to smaller water clusters,[13,14] emphasizing a probable change in the hydrogen bond network around this region, in which almost all water molecules are three-coordinated.[14] So, the change in the hydrogen bond network could be the one possible reason for the convergence of the appearance energy values for neutral water clusters greater than 20 molecules in our experiment.

There have been numerous theoretical determinations of water cluster ionization energy dependence on size.[53,58−62] Unfortunately, although there is a qualitative agreement with our measured energies, insofar as there is a monotonic decline in ionization energies with increasing cluster size, quantitatively there is not much agreement. This disagreement probably arises because the theoretical work typically reports energies for the lowest lying and most energetically stable conformers. In contrast, the experimental values represent an average ionization energy for the same cluster size, which includes a contribution from a large number of different conformers, especially when a relatively high internal temperature is anticipated for large water clusters in our molecular beam.

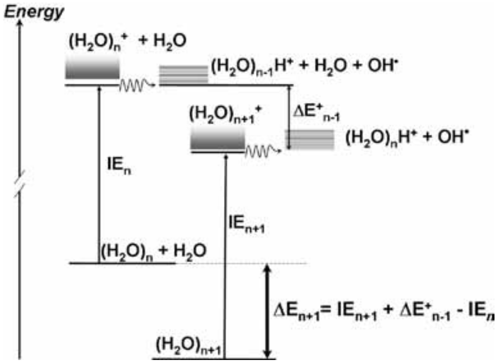

Figure 8. Schematic diagram of water cluster photoionization.

The experimental appearance energy measurements allow for the determination of the dissociation energy of a single water molecule loss from the parent neutral water cluster. A simple thermodynamic cycle shown in Figure 8, which utilizes the appearance energies, derived in this work, along with the energy for the single water molecule loss from protonated water clusters measured by Wang et al.[42] are used to evaluate the energy for one water molecule loss from neutral water clusters.

According to this diagram, the energy required to photoionize the ($n + 1$)-mer and n-mer neutral water clusters are denoted IE_{n+1} and IE_n, respectively, and represent the appearance energies of n-mer and ($n - 1$)-mer protonated water clusters, respectively, which are measured in this work. Using the diagram in Figure 8, the dissociation energy (ΔE_{n+1}) of one water molecule from the ($n + 1$)-mer neutral water cluster can be calculated using energy conservation, as shown in eq 3

$$\Delta E_{n+1} = \mathrm{IE}_{n+1} + \Delta E_{n-1}^{+} - \mathrm{IE}_n \qquad (3)$$

where IE_{n+1} and IE_n are the appearance energies of $(H_2O)_{n+1}$ and $(H_2O)_n$, respectively, and ΔE_{n-1}^{+} is the dissociation energy of one water molecule from the ($n - 1$)-mer protonated water cluster, as described in eq 2. The dissociation energy of smaller protonated water clusters $(H_2O)_3$ and $(H_2O)_4$ are calculated based on eq 3, employing an averaged value of ΔE_n^{+}, 138 ± 8 kJ/mol and 85 ± 6 kJ/mol, for $(H_2O)_2H^+$ and $(H_2O)_3H^+$, respectively.[63−67] The dissociation energies for larger neutral clusters, $3 \leq n \leq 9$, are calculated using the latest reported values for ΔE_n^{+}, by Wang et al.[42] The dissociation energies for larger protonated water clusters are reported by Shi et al.[28] and Magnera et al.[68] However, due to the large fluctuations in ΔE_n^{+} for protonated water clusters $7 \leq n \leq 28$, reported by Shi et al.[28] and Magnera et al.,[68] the final analysis would lead to large uncertainties in calculating ΔE_n and therefore, values for water molecule dissociation from $n > 9$ neutral water clusters are not reported here. Moreover, the difference of the appearance energy values (IE_n) for water clusters $n > 9$ are not significant (±0.2 eV, see Figure 7), suggesting that any calculations based on ΔE_n^{+} would be just a reflection of the protonated water cluster thermochemistry. It must be emphasized here that employing

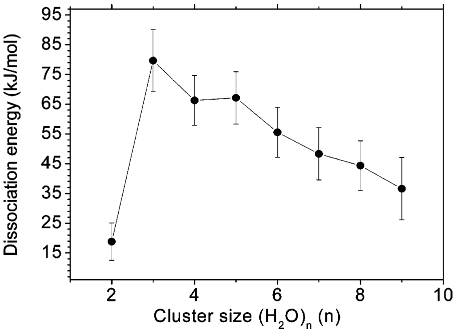

Figure 9. Neutral water cluster dissociation energies, for the process $(H_2O)_n \rightarrow (H_2O)_{n-1} + H_2O$.

TABLE 1: Experimental Values of Neutral Water Cluster Dissociation Energies for Single Water Molecule Loss: $(H_2O)_n \rightarrow (H_2O)_{n-1} + H_2O$

	dissociation energy (kJ/mol)	
cluster	this work	literature
$(H_2O)_2$	19 ± 6	15.3 ± 2.0[5]
$(H_2O)_3$	80 ± 10	
$(H_2O)_4$	66 ± 8	
$(H_2O)_5$	67 ± 9	
$(H_2O)_6$	56 ± 8	
$(H_2O)_7$	48 ± 8	
$(H_2O)_8$	44 ± 8	
$(H_2O)_9$	37 ± 10	

eq 3 for calculating the dissociation energy of neutral water clusters is based on the assumption that the protonated water clusters ($(H_2O)_{n-1}H^+$) are formed in their ground vibrational states. In addition we make the assumption in this analysis that intracluster proton transfer as well as OH loss retain their characteristic energies no matter whether the species is $(H_2O)_n^+$ or $(H_2O)_{n+1}^+$ clusters.

The dissociation energy of the neutral water dimer cannot be calculated by employing eq 3. However, it can be evaluated based on the proton affinity (PA) of water and the appearance energy of H_3O^+ from water dimer photoionization using eq 4

$$\Delta E_2 = \mathrm{AE}(\mathrm{H_3O^+}) + \mathrm{PA}(\mathrm{H_2O}) - \mathrm{AE}(\mathrm{H^+/H_2O}) \qquad (4)$$

where $\mathrm{AE}(\mathrm{H_3O^+}) = 11.74 \pm 0.05$ eV is the appearance energy for H_3O^+, $\mathrm{PA}(\mathrm{H_2O}) = 690$ kJ/mol is the proton affinity of water,[69] and $\mathrm{AE}(\mathrm{H^+/H_2O}) = 18.7$ eV is the appearance energy of H^+ from water photoionization.[70] Employing these numbers, the dissociation energy of the water dimer equals 19 ± 6 kJ/mol. The resulting dissociation energy values for neutral water clusters, as a function of size, are plotted in Figure 9, and the numerical values are shown in Table 1.

Among neutral water clusters, only the dissociation energy of the dimer has been tentatively evaluated, based on the spectroscopic studies of Fellers et al.[5] Our value, 19 ± 6 kJ/mol, is 4 kJ/mol higher but is consistent within the experimental error bars. The experimental values of ΔE_n for larger water clusters have not been reported before, to the best of our knowledge.

It is important to discuss the physical meaning of the dissociation energy dependence on neutral cluster size. The dissociation energy shows a remarkable increase in going from dimer to trimer. The main reason for this is the number and strength of hydrogen bonds (H-bonds). The dissociation of the dimer requires breaking of a single H-bond. In the case of the trimer, two H-bonds have to be broken, taking into account the most stable cyclic geometry. Moreover, based on ab initio calculations, the intracluster O−O distance between two neighboring oxygen atoms is noticeably shorter in the trimer, suggesting stronger bonding.[71]

The dissociation energy of a single water molecule from a larger neutral water cluster (beyond trimer) shows a gradual decrease as the cluster size increases. The most thermodynamically stable structure of small neutral water clusters ($3 \le n \le 5$) has a ring geometry. The dissociation of one water molecule from the trimer requires breaking of two H-bonds and only one H-bond remains in the cluster to make a stable dimer, revealed in the large difference in the dissociation energy, from 80 ± 10 to 19 ± 6 kJ/mol, for trimer and dimer, respectively. For the case of tetramer and pentamer, the dissociation of one water molecule requires the breaking of two H-bonds followed by cluster reorganization and formation of a new, weaker H-bond in the trimer or tetramer, respectively: 30.6, 29.0, and 21.6 kJ/mol for pentamer, tetramer and trimer, respectively.[72] Therefore, water molecule dissociation from the cyclic trimer is more endothermic than from the other larger cyclic structures. Larger clusters have more complicated 3D structures and water molecule loss requires more than two H-bonds to break and form. For example, the predominant geometry of the water hexamer in the gas phase is a cage like structure.[73] In order to convert the cage structure, following the dissociation of one water molecule, and creating a cyclic pentamer, the rearrangement of more than two H-bonds has to be considered.

According to the theoretical calculations of Su et al.,[72] the H-bonding strength increases as a function of the water cluster size, from the dimer to the pentamer and then decreases to the bulk ice value of 23.8 kJ/mol for clusters larger than the hexamer. However, there is not a strict correspondence between the H-bonding strength and the dissociation energy for one water molecule from a neutral cluster since these neutral water clusters ($n > 5$) have more than one H-bond per water monomer.

Conclusions

In this paper we demonstrate, for the first time, an experimental evaluation of neutral water cluster appearance energies, for $2 \le n \le 80$ water molecules and the dissociation energies for loss of a single water monomer from the neutral water cluster ($2 \le n \le 9$) in a supersonic molecular beam. The decrease of the protonated water cluster ion appearance energy values as a function of cluster size for $n < 20$ is probably a manifestation of the stabilization of the overall cluster geometry and intracluster hydrogen-bonding network. The appearance energies of clusters larger than 20 water molecules converge to 10.6 eV. Photoionization studies of gas-phase water clusters provide a window to quantify the hydrogen bond network in water.

Acknowledgment. We thank M. A. Duncan and E. R. Bernstein for helpful discussions and D. S. Peterka and M. Jimenez-Cruz for help at the beamline. This work was supported by the Director, Office of Energy Research, Office of Basic Energy Sciences, Chemical Sciences Division of the U.S. Department of Energy under Contract No. DE-AC02-05CH11231.

Supporting Information Available: Table of the size dependent appearance energies of neutral water cluster $(H_2O)_n$, derived from the appearance energy observations of protonated water clusters (Table A). This material is available free of charge via the Internet at http://pubs.acs.org.

References and Notes

(1) Nilsson, A.; Wernet, P.; Nordlund, D.; Bergmann, U.; Cavalleri, M.; Odelius, M.; Ogasawara, H.; Naslund, L. A.; Hirsch, T. K.; Glatzel, P.; Pettersson, L. G. M. *Science* **2005**, *308*, 793a.

(2) Smith, J. D.; Cappa, C. D.; Messer, B. M.; Cohen, R. C.; Saykally, R. J. *Science* **2005**, *308*, 793b.

(3) Smith, J. D.; Cappa, C. D.; Wilson, K. R.; Messer, B. M.; Cohen, R. C.; Saykally, R. J. *Science* **2004**, *306*, 851−853.

(4) Wernet, P.; Nordlund, D.; Bergmann, U.; Cavalleri, M.; Odelius, M.; Ogasawara, H.; Naslund, L. A.; Hirsch, T. K.; Ojamae, L.; Glatzel, P.; Pettersson, L. G. M.; Nilsson, A. *Science* **2004**, *304*, 995−999.

(5) Fellers, R. S.; Leforestier, C.; Braly, L. B.; Brown, M. G.; Saykally, R. J. *Science* **1999**, *284*, 945−948.

(6) Liu, K.; Cruzan, J. D.; Saykally, R. J. *Science* **1996**, *271*, 929−933.

(7) Cruzan, J. D.; Braly, L. B.; Liu, K.; Brown, M. G.; Loeser, J. G.; Saykally, R. J. *Science* **1996**, *271*, 59−62.

(8) Pugliano, N.; Saykally, R. J. *Science* **1992**, *257*, 1937−1940.

(9) Yeh, L. I.; Lee, Y. T.; Hougen, J. T. *J. Mol. Spectrosc*. **1994**, *164*, 473−488.

(10) Vernon, M. F.; Krajnovich, D. J.; Kwok, H. S.; Lisy, J. M.; Shen, Y. R.; Lee, Y. T. *J. Chem. Phys.* **1982**, *77*, 47−57.

(11) Ahmed, M.; Apps, C. J.; Hughes, C.; Whitehead, J. C. *J. Phys. Chem.* **1994**, *98*, 12530−12534.

(12) Brundle, C. R.; Turner, D. W. *Proc. R. Soc. London, A* **1968**, *307*, 27−36.

(13) Shin, J. W.; Hammer, N. I.; Diken, E. G.; Johnson, M. A.; Walters, R. S.; Jaeger, T. D.; Duncan, M. A.; Christie, R. A.; Jordan, K. D. *Science* **2004**, *304*, 1137−1140.

(14) Miyazaki, M.; Fujii, A.; Ebata, T.; Mikami, N. *Science* **2004**, *304*, 1134−1137.

(15) Lin, S. S. *Rev. Sci. Instrum.* **1973**, *44*, 516−517.

(16) Searcy, J. Q.; Fenn, J. B. *J. Chem. Phys.* **1974**, *61*, 5282−5288.

(17) Eigen, M. *Angew. Chem. Int. Ed.* **1964**, *3*, 1−19.

(18) Zundel, G. *The Hydrogen Bond* − *Recent Developments in Theory and Experiments. II. Structure and Spectroscopy*; North-Holland: Amsterdam, 1976; Vol. 2, pp 683−766.

(19) Vostrikov, A. A.; Dubov, D. Y. *Z. Phys. D: At., Mol. Clusters* **1991**, *20*, 429−432.

(20) Torchet, G.; Schwartz, P.; Farges, J.; Deferaudy, M. F.; Raoult, B. *J. Chem. Phys.* **1983**, *79*, 6196−6202.

(21) Schreiner, J.; Voigt, C.; Kohlmann, A.; Amold, F.; Mauersberger, K.; Larsen, N. *Science* **1999**, *283*, 968−970.

(22) Cho, J. Y. N.; Rottger, J. *J. Geophys. Res. [Atmos.]* **1997**, *102*, 2001−2020.

(23) Dong, F.; Heinbuch, S.; Rocca, J. J.; Bernstein, E. R. *J. Chem. Phys.* **2006**, *124*, 224319.

(24) Ng, C. Y.; Trevor, D. J.; Tiedemann, P. W.; Ceyer, S. T.; Kronebusch, P. L.; Mahan, B. H.; Lee, Y. T. *J. Chem. Phys.* **1977**, *67*, 4235−4237.

(25) Shinohara, H.; Nishi, N.; Washida, N. *J. Chem. Phys.* **1986**, *84*, 5561−5567.

(26) Shiromaru, H.; Shinohara, H.; Washida, N.; Yoo, H. S.; Kimura, K. *Chem. Phys. Lett.* **1987**, *141*, 7−11.

(27) Nagashima, U.; Shinohara, H.; Nishi, N.; Tanaka, H. *J. Chem. Phys.* **1986**, *84*, 209−214.

(28) Shi, Z.; Ford, J. V.; Wei, S.; Castleman, A. W. *J. Chem. Phys.* **1993**, *99*, 8009−8015.

(29) Wei, S. Q.; Castleman, A. W. *Int. J. Mass Spectrom. Ion Processes* **1994**, *131*, 233−264.

(30) Radi, P. P.; Beaud, P.; Franzke, D.; Frey, H. M.; Gerber, T.; Mischler, B.; Tzannis, A. P. *J. Chem. Phys.* **1999**, *111*, 512−518.

(31) Hammer, N. I.; Shin, J. W.; Headrick, J. M.; Diken, E. G.; Roscioli, J. R.; Weddle, G. H.; Johnson, M. A. *Science* **2004**, *306*, 675−679.

(32) Verlet, J. R. R.; Bragg, A. E.; Kammrath, A.; Cheshnovsky, O.; Neumark, D. M. *Science* **2005**, *307*, 93−96.

(33) Bragg, A. E.; Verlet, J. R. R.; Kammrath, A.; Cheshnovsky, O.; Neumark, D. M. *Science* **2004**, *306*, 669−671.

(34) Hammer, N. I.; Roscioli, J. R.; Bopp, J. C.; Headrick, J. M.; Johnson, M. A. *J. Chem. Phys.* **2005**, *123*, 224311.

(35) Tachikawa, H. *J. Phys. Chem. A* **2004**, *108*, 7853−7862.

(36) Jongma, R. T.; Huang, Y. H.; Shi, S. M.; Wodtke, A. M. *J. Phys. Chem. A* **1998**, *102*, 8847−8854.

(37) Klots, C. E. *J. Chem. Phys.* **1985**, *83*, 5854−5860.

(38) Richard-Viard, M.; Delboulbe, A.; Vervloet, M. *Chem. Phys.* **1996**, *209*, 159−167.

(39) Nicolas, C.; Shu, J.; Peterka, D. S.; Hochlaf, M.; Poisson, L.; Leone, S. R.; Ahmed, M. *J. Am. Chem. Soc.* **2006**, *128*, 220−226.

(40) Lancaster, G. M.; Honda, F.; Fukuda, Y.; Rabalais, J. W. *J. Am. Chem. Soc.* **1979**, *101*, 1951−1958.

(41) Klots, C. E. *Nature* **1987**, *327*, 222−223.

(42) Wang, Y. S.; Tsai, C. H.; Lee, Y. T.; Chang, H. C.; Jiang, J. C.; Asvany, O.; Schlemmer, S.; Gerlich, D. *J. Phys. Chem. A* **2003**, *107*, 4217−4225.

(43) James, T.; Wales, D. J.; Hernandez-Rojas, J. *Chem. Phys. Lett.* **2005**, *416*, 302−307.

(44) James, T.; Wales, D. J. *J. Chem. Phys.* **2005**, *122*, 134306.

(45) Liu, K.; Brown, M. G.; Saykally, R. J. *J. Phys. Chem. A* **1997**, *101*, 8995−9010.

(46) Mella, M.; Clary, D. C. *J. Chem. Phys.* **2003**, *119*, 10048−10062.

(47) Chang, H. C.; Wu, C. C.; Kuo, J. L. *Int. Rev. Phys. Chem.* **2005**, *24*, 553−578.

(48) Narten, A. H.; Danford, M. D.; Levy, H. A. *Discuss. Faraday Soc.* **1967**, 97−107.

(49) Narten, A. H.; Thiessen, W. E.; Blum, L. *Science* **1982**, *217*, 1033−1034.

(50) Fletcher, N. H. *The Chemical Physics of Ice*; Cambridge University Press: Cambridge, 1970.

(51) Eisenberg, D.; Kauzmann, W. *The Structure and Properties of Water*; Oxford University Press: Oxford, 1969.

(52) Venkatesh, C. G.; Rice, S. A.; Narten, A. H. *Science* **1974**, *186*, 927−928.

(53) Barnett, R. N.; Landman, U. *J. Phys. Chem. A* **1997**, *101*, 164−169.

(54) Furuhama, A.; Dupuis, M.; Hirao, K. *J. Chem. Phys.* **2006**, *124*, 164310.

(55) Hermann, V.; Kay, B. D.; Castleman, A. W. *Chem. Phys.* **1982**, *72*, 185−200.

(56) Nauta, K.; Miller, R. E. *Science* **2000**, *287*, 293−295.

(57) Winter, B.; Weber, R.; Widdra, W.; Dittmar, M.; Faubel, M.; Hertel, I. V. *J. Phys. Chem. A* **2004**, *108*, 2625−2632.

(58) Muller, I. B.; Cederbaum, L. S. *J. Chem. Phys.* **2006**, *125*, 204305.

(59) Novakovskaya, Y. V.; Stepanov, N. F. *J. Phys. Chem. A* **1999**, *103*, 3285−3288.

(60) Tomoda, S.; Kimura, K. *Chem. Phys. Lett.* **1983**, *102*, 560−564.

(61) do Couto, P. C.; Cabral, B. J. C. *J. Chem. Phys.* **2007**, *126*, 014509.

(62) Woon, D. E. *Adv. Space Res.* **2004**, *33*, 44−48.

(63) Meotner, M.; Speller, C. V. *J. Phys. Chem.* **1986**, *90*, 6616−6624.

(64) Meotner, M.; Field, F. H. *J. Am. Chem. Soc.* **1977**, *99*, 998−1003.

(65) Kebarle, P.; Searles, S. K.; Zolla, A.; Scarboro, J.; Arshadi, M. *J. Am. Chem. Soc.* **1967**, *89*, 6393−6399.

(66) Cunningham, A. J.; Payzant, J. D.; Kebarle, P. *J. Am. Chem. Soc.* **1972**, *94*, 7227−7632.

(67) Wroblewski, T.; Ziemczonek, L.; Gazda, E.; Karwasz, G. P. *Radiat. Phys. Chem.* **2003**, *68*, 313−318.

(68) Magnera, T. F.; David, D. E.; Michl, J. *Chem. Phys. Lett.* **1991**, *182*, 363−370.

(69) Hunter, E. P. L.; Lias, S. G. *J. Phys. Chem. Ref. Data* **1998**, *27*, 413−656.

(70) Appell, J.; Durup, J. *Int. J. Mass Spectrom. Ion Phys.* ***1973***, *10*, 247.

(71) Keutsch, F. N.; Cruzan, J. D.; Saykally, R. J. *Chem. Rev.* **2003**, *103*, 2533−2577.

(72) Su, J. T.; Xu, X.; Goddard, W. A. *J. Phys. Chem. A* **2004**, *108*, 10518−10526.

(73) Liu, K.; Brown, M. G.; Carter, C.; Saykally, R. J.; Gregory, J. K.; Clary, D. C. *Nature* **1996**, *381*, 501−503.